Ligand excess 'inverse-defected' Zr_6 tetrahedral tetracarboxylate framework, and its thermal transformation

Bahareh Nateghi,[a] Konstantin V. Domasevitch,[b] Roman Bulánek,[c] Christoph Janiak*[a], Ishtvan Boldog*[c]

[a] *Institute of Inorganic Chemistry and Structural Chemistry, Heinrich-Heine-Universität Düsseldorf, Universitätsstr. 1, D-40225 Düsseldorf, Germany.*
[b] *Inorganic Chemistry Department, Taras Shevchenko National University of Kiev, Vladimirskaya Street 64, Kiev 01033, Ukraine*
[c] *University of Pardubice, Faculty of Chemical Technology, Department of Physical Chemistry, Studentská 573,532 10 Pardubice, Czech Republic.*

E-mails: ishtvan.boldog@gmail.com, janiak@uni-duesseldorf.de

Keywords: zirconium, adamantane, tetrahedral, truncate, flu, MOF, porous, mixed ligand.

† Supplementary Information (SI) available: additional notes concerning the synthesis, solution and refinement of the single crystal XRD structure, PXRD-based structure verification, PXRD data, TG-DTA, gas adsorption experiments, ^{1}H NMR and IR spectra.

Abstract

A new porous coordination polymer (PCP/MOF), **ZRTE-10**,§ based on a tetrahedral 1,3,5,7-tetra(carboxyphenyl)benzene ligand (H_4L^4) was synthesized using formic or acetic acids as modulators. The low symmetry (*C*2/c) framework, $[Zr_6(\mu_3\text{-}O)_4(\mu_3\text{-}OH)_4(L^4)(HL^4)_2(OH)_2(H_2O)_2]$, is built upon a rare 10-connected Zr_6 cluster. Two third of the ligands bear one non-deprotonated carboxy group, and the framework has a complex trinodal 3,4,10-c, $\{4^{14}.6^{24}.8^7\}\{4^3\}_2\{4^5.6\}$ underlying net. Supercritical CO_2 drying and mild degassing at 120 °C yielded a porous material with S_{BET} = 1190 m^2 g^{-1}. When heated up to ~200 °C **ZRTE-10** converts to another crystalline framework, **ZRTE-11**.§ The latter was identified to be identical to the expected fluorite (**flu**) observed previously for other tetrahedral ligands. The high symmetry (*I*4/m) is built upon 8-connected Zr_6 clusters and has a formula of $[Zr_6(\mu_3\text{-}O)_4(\mu_3\text{-}OH)_4(OH)_4(L^4)_2]$. The complicated trinodal network of **ZRTE-10** and the simple **flu** net in **ZRTE-11** are topologically interrelated *via* the operation of merging of two neighbor three-connected nodes to one four-connected. The thermally induced conversion of **ZRTE-10** undergoes with expulsion of one ligand per Zr_6 node in the pores of the framework, resulting in a relatively low S_{BET} = 585 m^2 g^{-1} for the activated H_4L^4@**ZRTE-11**. Mixed ligand approach for **ZRTE-10,11** was attempted *via* using 1,3,5-tetra(carboxyphenyl)benzene (H_3L^3), which is a truncated analog of H_4L^4 with one missing branch. The monocrystalline sample of **ZRTE-10** obtained in small yields demonstrated only minor inclusion of H_3L^3. However, the high-yielding (~80%) procedure with HCl as a modulator allows near proportional incorporation of the ligands. The formed materials are semi-amorphous with powder XRDs intermediary between pure **ZRTE- 10** and **11**. Thermal

treatment of the semi-amorphous materials increases their crystallinity and allows to reach S_{BET} = 400-550 m^2 g^{-1} surface areas for pure H_4L^4 and H_3L^3 or their mixture alike. The approach proposes viewpoint on the H_3L^3 trifunctional ligand as a model of a ligand platform, suitable for bearing a large functionality on the place of the fourth 'truncated' branch. The significance of **ZRTE-10** as a material for postsynthetic introduction of metal-based cluster functionality and as a model of functionality-encapsulation, an alternative to ship-in-the-bottle method, is discussed.

Introduction

Porous coordination polymers (PCP), also known as metal-organic frameworks (MOFs) are porous crystalline compounds consisting of metal ions or clusters interconnected by organic ligands. Zirconium carboxylates[1] are an important subclass of PCPs possessing an infrequent combination of high porosity, considerable thermal and hydrolytic/chemical stability, low toxicity, optical transparency and diamagnetism (important for use as matrixes for hosting active species) and not prohibitive price. Indeed, most of the potential applications for PCPs typically consider zirconium carboxylates among the most promising candidates. Typical applications are small molecule storage,[2,3] separation,[4,5,6] and delivery[7] as well as catalysis[8, 9 ,10,11,12] and sensorics.[13,14]

The structural predictability of zirconium carboxylates is a feature, highly valued in PCP research. It is associated with the high stability of the $\{Zr_6(\mu_3\text{-}O)_4(\mu_3OH)_4(RCOO)_{12}\}$ cuboctahedral cluster (Fig. 1) and its carboxylate-incomplete variants. The reticular chemistry approach is highly suitable for this class of compounds, comparable to the much less stable zinc carboxylates. The prototypal structural types are reproduced after functionalization of the ligands by a broad range of groups, including potential ligating moieties like amino-,[15] hydroxy-,[16] sulphonic acid,[17] carboxylic acid,[18] bipyridyl [19] etc., as well as so bulky fragments as a *n*-membered macrocycle.[20] The geometric scalability of the ligands is also one of the best for the known isoreticular series (the classical $\{Zn(O)(RCOO)_6\}$-based MOF-5 type IRMOF series,[21] is the classical competitor with properties often plagued by interpenetration; the $\{[Mg(R'O)(RCOO)]_\infty\}$ based IRMOF-74-*n* series[22] is unique regarding the extent of possible ligand elongation; some $\{M_3(O)(X)(RCOO)_6\}$-based series, particularly of the MIL-88 type, have an apparent potential,[23,24] which is yet to be fully disclosed). The availability of an isoreticular series with a large number of representatives makes it possible to focus on the functional side of material's design and invest less time in fundamental structural aspects.

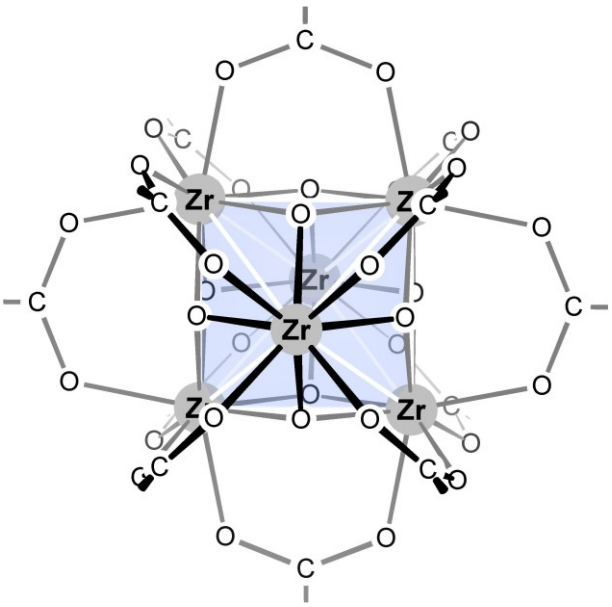

Fig. 1 The $\{Zr_6(OH)_4(O)_4(COOH)_{12}\}$ cluster.

The three most important isoreticular series are based on: a) linear ligands, yielding mostly compounds with **fcu** underlying net or its subnets (UiO-66 type [15]); b) square-shaped ligands[25] yielding the **ftw** net; c) regular-tetrahedral ligands[26] producing the **flu** net.[1] In these cases the ligands are perfectly compatible with the $\{Zr_6(\mu_3\text{-}O)_4(\mu_3\text{-}OH)_4(RCOO)_{12-n}(OH)_n(H_2O)_n\}$ cluster, ensuring connectivity ranging from 12 (cuboctahedral unit) to 8 (typically a cubic unit) to be combined in periodic nets close to their most symmetric representations. Important to note, that despite the excellent matching of prerequisites for formation of highly symmetric compounds, there are alternatives, primarily because of easy geometric deformations either on the side of the ligand or the cluster. The realization of alternative types is typical for square ligands, e.g. in the cases of PCN-222[27] (**csq**), PCN-224 (**she**),[28] PCN-225(**sqc**)[29] and 'exceptions' are dominant for regular triangular- shape ligands with like MOF-808 (**spn**),[30] PCN-777[31] (β-crystobalite) and UMCM-309 [32] (**kgd**). All the listed cases are based on the Zr_6 cluster; PCPs based on other secondary building units are of lesser importance (even if some highly symmetric alternatives are known, like the Zr_8 cubic cluster [33]);[1] notable exception is the MIL-140 series[34].

The variability in number of the carboxylate groups in the $\{Zr_6(\mu_3\text{-}O)_4(\mu_3\text{-}OH)_4(RCOO)_{12-n}(OH)_n(H_2O)_n\}$, where n = 0-4 are the number of 'defects', allows the adjustment of connectivity of the Zr_6 cluster ('capping' terminal carboxylates are an alternative to pairs of OH and H_2O terminal ligands). In high-connectivity Zr-PCPs a part of the linker ligands could be missing to form defects,[35] which in the case of UiO-66 could be so numerous that the two limiting cases featuring 4 missing carboxylates are practically different compounds, as in the case of defect poor (with **fcu** topology) and defect-rich UiO-66 (e.g. with **reo** topology).[36,37] The eliminated carboxylic acids leave coordinatively unsaturated sites (CUS-es),[10] which are 'dockable' not only by carboxylic acids but a range variety of other species

(for example, vanadium acetylacetonate was docked for gas-phase catalysis of the oxidative dehydrogenation of cyclohexane[38]). The Lewis acidity of the CUS-es,[39] which could be tuned even to form species resembling the active sites in the well-known sulfated-zirconia,[40] as well as possibilities for introduction of ligand based basicity,[41] explains the interests to Zr-MOFs as potential catalysts,[9] especially for the synthesis of organic compounds performed under mild conditions.[42,43,44]

Introduction of defects in PCPs is the more feasible, the more highly connected the network is, due to lowering the impact of a single linker on network stability. Coordination bonded clusters could easily ensure much higher connectivities than the organic connectors and are easily accessible. The $\{Zr_6(\mu_3\text{-}O)_4(\mu_3OH)_4(RCOO)_{12}\}$ cluster is an example of a secondary building block (SBU) of highest connectedness and its prominence in 'defect-engineered' PCPs is not surprising. However, the level of control on the cluster-based defects is relatively low as they are self-assembling during the synthesis.

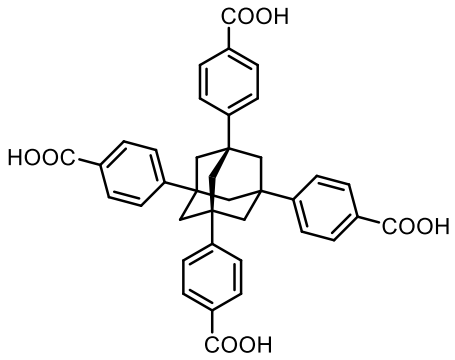

H_4L^4

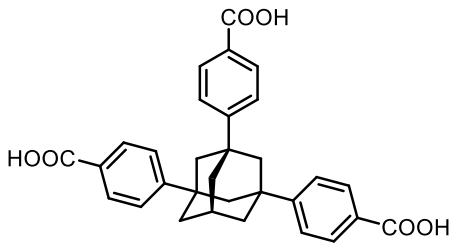

H_3L^3

Fig. 2 The H_4L^4 and H_3L^3 ligands.

An inverse strategy for defect introduction is the truncation of the ligand.[45,46,47] The truncated site could potentially be functionalized, while ultimate control could be exercised as the synthesis of the ligand precedes the last step of the PCP's self-assembly. Provided that the connectedness of the cluster is high, the ligand-candidate for truncation might have relatively low branching (potentially it could be a pair of a bifunctional linker and its monofunctional 'half', however high lability and lowered incorporation control makes such approach *apriori*

disadvantaged). However, high connectedness of the ligand is favorable for overall mechanical stability and preservation of maximal similarity between the prototypal- and truncated ligands. The connectivity of at least four as well as the non-planar geometry seems to be sufficient and is the obvious choice in the case of Zr-MOFs is the truncation of tetrahedral ligands. Recently, we have explored the crystallization outcomes for complete and 'truncated' adamantane based tetrahedral ligands and have found that the self-assembly is strongly symmetry driven (see ref. and also the discussion herein).[46] To explore potential defect-creation strategies a compound class with strictly defined cluster-type should be chosen (i.e. a 'cluster-driven' self-assembly approach) and Zr-MOFs meet this demand very well.

The first two Zr-PCPs with tetrahedral ligands were first reported almost simultaneously by Furukawa *et al.* [30] and Zhang *et al.* [26] in 2014. A small ((methanetetrayl)tetrakis-(phen-1,4-ylene)) tetracarboxylic acid (H_4MTB) and its larger homolog, ((methanetetrayl)tetrakis-(biphen-4,4'-diyl)) tetracarboxylic acid (H_4MTBC) were used respectively. We have chosen 1,3,5,7-tetraphenyladamantane as a tetrahedral platform, which has a size between tetraphenylmethane and its phenyl-expanded, tetrakis(biphenyl)methane homologue used in this role before. The primary reason for using a yet unreported platform was the synthetic accessibility of all the bridgehead substituted oligophenyladamantanes by the same "Newman's route",[48] and the assuredness that the respective isoreticular compound with **flu** net topology based on the tetrahedral ligand should exist. Accordingly, we aimed the investigation of the((adamantane-1,3,5,7-tetrayl)tetra(phen-4-yl))tetracarboxylic acid, H_4L^4, and its 'truncated' analogue, the ((adamantane-1,3,5-triyl)tri(phen-4-yl))tricarboxylic acid, H_3L^3, as a building block pair for special ligand-based introduction of defects (Fig. 2). The results were only partially expected and the curios implications are reported in this contribution.

Results and discussion

$[Zr_6(\mu_3\text{-}O)_4(\mu_3\text{-}OH)_4(L^4)(HL^4)_2(OH)_2(H_2O)_2] \cdot 4\ DMF \cdot 2\ HCOOH \cdot 4\ H_2O$; 1 (phase I). Attempts to synthesize Zr-PCPs by reacting $ZrOCl_2 \cdot 8H_2O$ or $ZrCl_4$ and the H_4L^4 or H_3L^3 ligands in DMF at 80-150 °C did not lead to products consisting of single crystals.[46] The syntheses were modified by the addition of typical modulators [26,1], including formic, acetic, benzoic acids and HCl (SI.1, i.e. chapter 6 of the Supplementary Information).‖ Pure phases, consisting of very small, but well-formed single crystals were obtained only in the case of the H_4L^4 ligand, when formic or acetic acid was used; the large used quantities of the modulators were essential (Fig. 3). The obtained I-HCOOH-as and I-AcOH-as materials were proven to be nearly identical (see the footnote § for naming conventions). Interestingly, the crystallinity of the samples significantly improved upon the use of a mixture of H_4L^4 with a small additive of H_3L^3, as low as 3%$_{mol}$. Significant increase of the H_3L^3's share eventually led to decrease

of crystallinity and the already low yield (10-20%; Table S1,2). While the use of acetic acid led to higher yields (~ 40%), formic acid ensured slightly better crystallinity, particularly evident during the single crystal XRD determination, and was used for scaled-up syntheses of material **1** (= I-HCOOH-as, synthesis with 3% of H_3L^3; **ZRTE-10** is the given framework code for external referencing [§]; see also Fig. 3**)**.

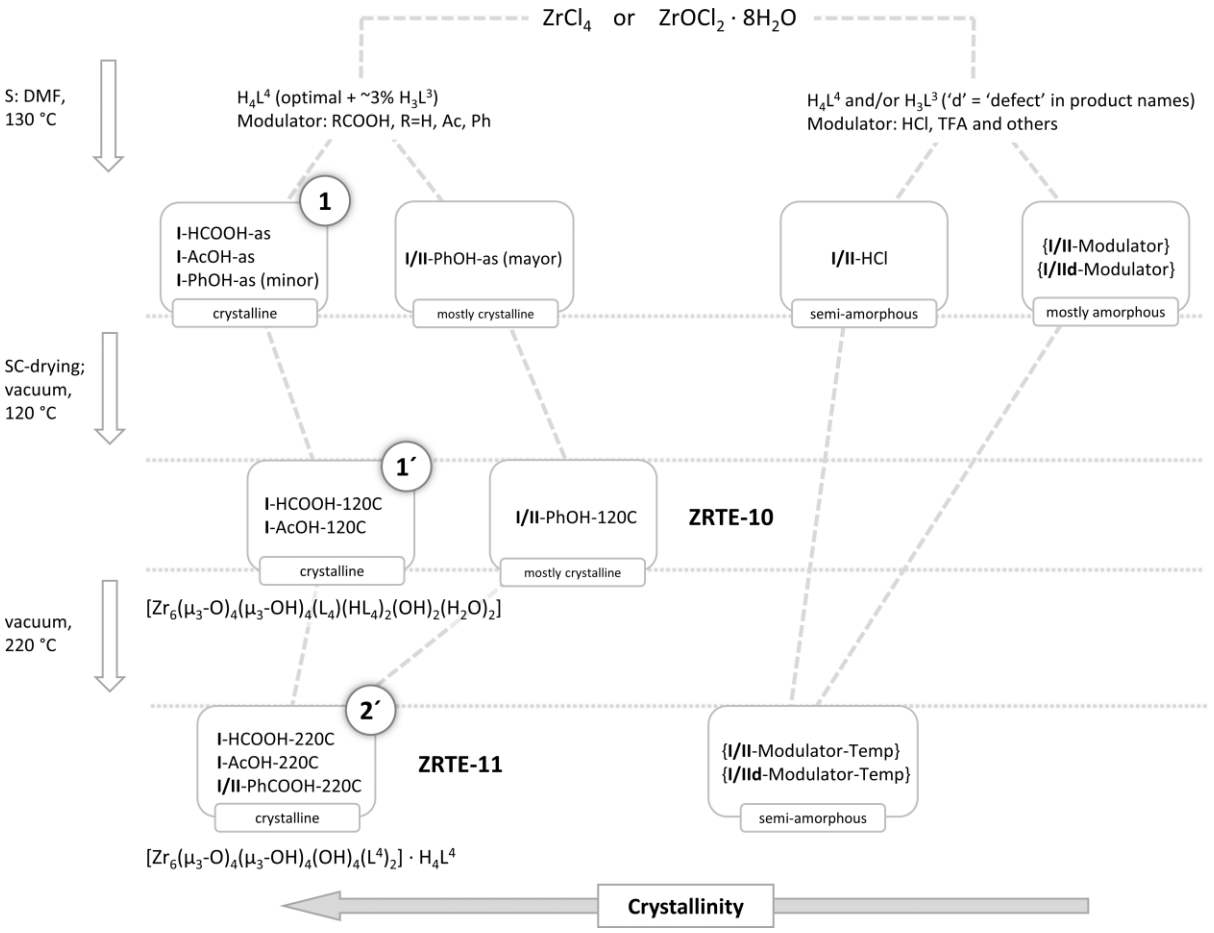

Fig. 3 Scheme of the synthesis and the transformations of the products at elevated temperatures (the ´-modifier stands for 'degassed'; the framework formulas are given with minimal level of dehydration).

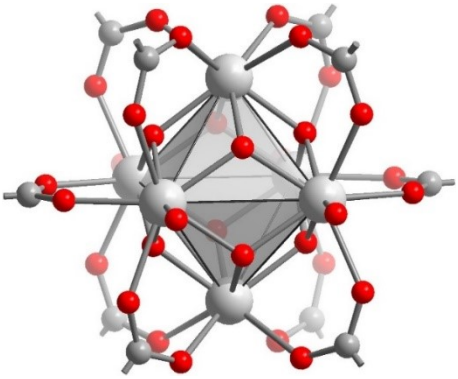

Fig. 4 The Zr_6 cluster in **1**, serving the role of a 10-c node of the framework (H-atoms are not shown for clarity; the positions of the oxygen atoms belonging to the O/OH ligands are averaged).

Single crystal X-ray diffraction study (SCXRD) of the crystals of **1**[&] (Fig. S1) established a framework structure with a composition of $[Zr_6(\mu_3\text{-}O)_4(\mu_3\text{-}OH)_4(L^4)(HL^4)_2(OH)_2(H_2O)_2]$ (the solvent content of the air-dried compound – 4 DMF, 2 HCOOH, and 4 H_2O per formula unit – was derived via TGA, see SI.6). The framework features the characteristic Zr_6 cluster (Fig. 4) with a connectivity of 10 (which is equal to the number of coordinated carboxylates). This value is unusual, compared to the typical value of 8 or 12, and to the best of our knowledge[1] there are only two well-documented Zr_6 based MOF structures with such connectivity: the MOF-802 [30] and DUT-69 [49]. These two structures are based on slightly bent 'pseudo-linear' ligands and overall are essentially different to **1**. Unlike the 'complete' octahedral cluster with 12 carboxylates, **1** does not feature one pair of bridging carboxylates, disposed in the equatorial plane and opposing each other. The respective coordination positions are filled with terminal *O*-ligands (Fig. 4, 5, S4). The analysis of the residual densities in the high-quality single crystal structure indicates that the coordinated oxygen atoms are isolated (in other words, the presence of site-sharing formate or DMF molecules is minimal). As the Zr-O bond-lengths involving the terminal *O*-ligands are of relevant difference, 2.1796(16) and 2.2146(6) Å, they were interpreted as belonging to hydroxido- and aqua-ligands respectively (SI.2). In this case the Zr_6 cluster has an equal number of μ_3-O and μ_3-OH ligands (4/4). This symmetric realization is the most typical for Zr_6 clusters, even if further deprotonation of the μ_3-OH ligands are possible. While bridging formate might be viewed as a more beneficial 'capping' ligand compared to a pair of hydroxido- and aqua ligands, both situations are common. Terminal formates are observed for example in the case of MOF-841, while hydroxido ligands in PCN-521,[26] or in a number of compounds featuring less than 12 carboxylates per cluster.[50]

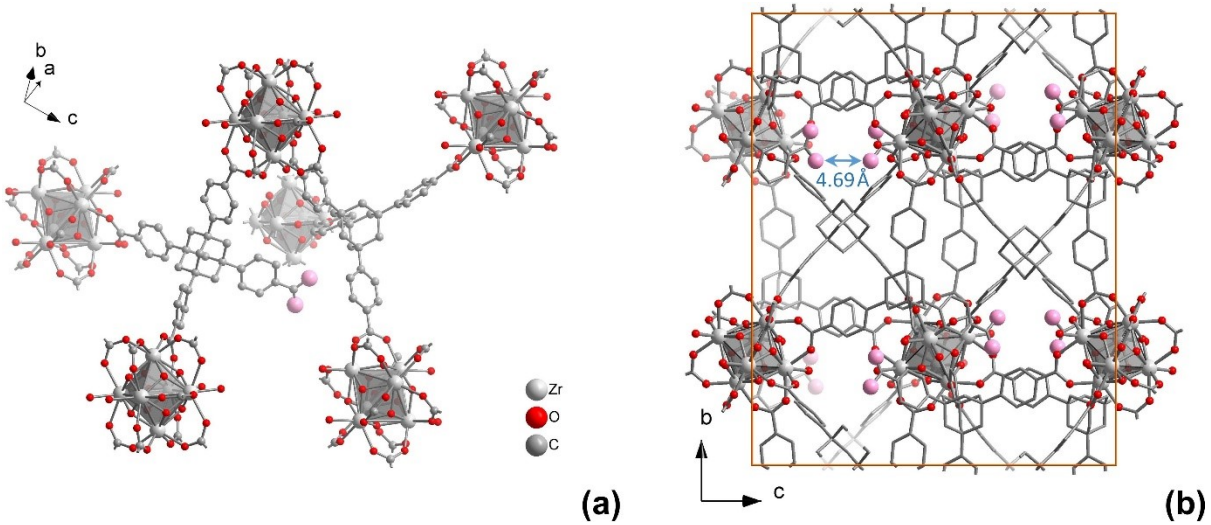

Fig. 5 (a) A representative fragment of the structure of **1**, demonstrating the μ_8-$(L^4)^{4-}$ and μ_6-$(HL^4)^{3-}$ ligands. The oxygen atoms of non-coordinated carboxylic acid functionality of μ_6-$(HL^4)^{3-}$ are shown in pink.
(b) The unit cell of the structure of **1**. Note the close disposition of the non-coordinated carboxylic acid functionalities (indicated by an arrow).

The hydrogen atoms are not shown for clarity; the oxygen atoms of μ_3-O and μ_3-OH are averaged.

Evidently, the framework structure of **1**, based on the 10-c node (-c stands for connectedness), is not equivalent topologically to the potentially expected **flu** net (which allows attaining $Fm\bar{3}m$ symmetry for a combination of a regular cubic and a regular tetrahedral building blocks). The 8-c node embodied by the most incomplete version of the Zr_6 cluster (4 missing carboxylates 'defects') on one hand and the 4-c node represented by a CR_4 or adamantane platforms on the other possesses the necessary symmetry. The structures of the known MOF-841 [30] and PCN-521 [26] follow that scenario; however, they demonstrate lower symmetry ($I4/m$) than the maximally possible. The distortions of the structure are obligatory for the realization of the **flu** net (it is enough to tell here, that the reason is that the carboxylate group is not a geometric point. Its bonding requirements is in conflict with the highest symmetry realization). The PCN-521 was the first structure of this type and the authors were eager to recognize the importance of the distortions. Due to the evidently strong bent of the long biphenyl 'branches' of the ligand (D_{2d} symmetry, instead of T_d; *cf.* D_{2h} max *vs* O_h symmetry for the Zr_6 cluster in **1** and in UiO-66 type structure) they even concluded that structure with a **flu** underlying net cannot be obtained for a smaller ligand.[26] This conjecture was proven wrong with the publication of the MOF-841[30] based on a minimal tetraphenylmethane core. Indeed, the distortions should not be necessarily associated with the bending of the ligand branches.

The necessary symmetry lowering in the real structures with **flu** underlying net is a subtle indication that alternative structures might not be rare. At least, they might be more expected, than the deviation from the maximum symmetry in the UiO-66 type (**fcu**), where the maximal symmetry ($Fm\bar{3}m$) is well compatible with the linear dicarboxylates. Notably, even in the latter case, such deviation occurs, and other topologies with 12-c Zr_6 clusters exist, as in the case of MOF-812 (**ith,** $C2/c$ actualization) [30]. It seems, that up to now the only well-known observed alternative to **fcu** is the highly porous NPF-200[51] (β-UH_3-like topology, high symmetry $Pm\bar{3}n$ actualization), which is an alternative product to PCN-521 (it is worth noting, however, that this trinodal network features also Zr_8 along with the Zr_6 cluster).

Thus, **1**, instead of **flu**, adopts a topology of a complex three-nodal underlying net with a stoichiometry of {HL^4-node: 3-c}{L^4-node: 4-c}$_2${Zr_6-node: 10-c} and, respectively, a point symbol of $\{4^{14}.6^{24}.8^7\}\{4^3\}_2\{4^5.6\}$ (see Table 1). Unlike in NPF-200, the deviation from the simplest binodal **flu** topology proceeded to two different ligand nodes instead of two metal cluster nodes. The 10-c Zr_6 cluster coordinate 2×3 carboxylates of the triply deprotonated ligand and 4 carboxylates of the fully deprotonated ligand (Fig. 5; see also Fig. 6b, left).

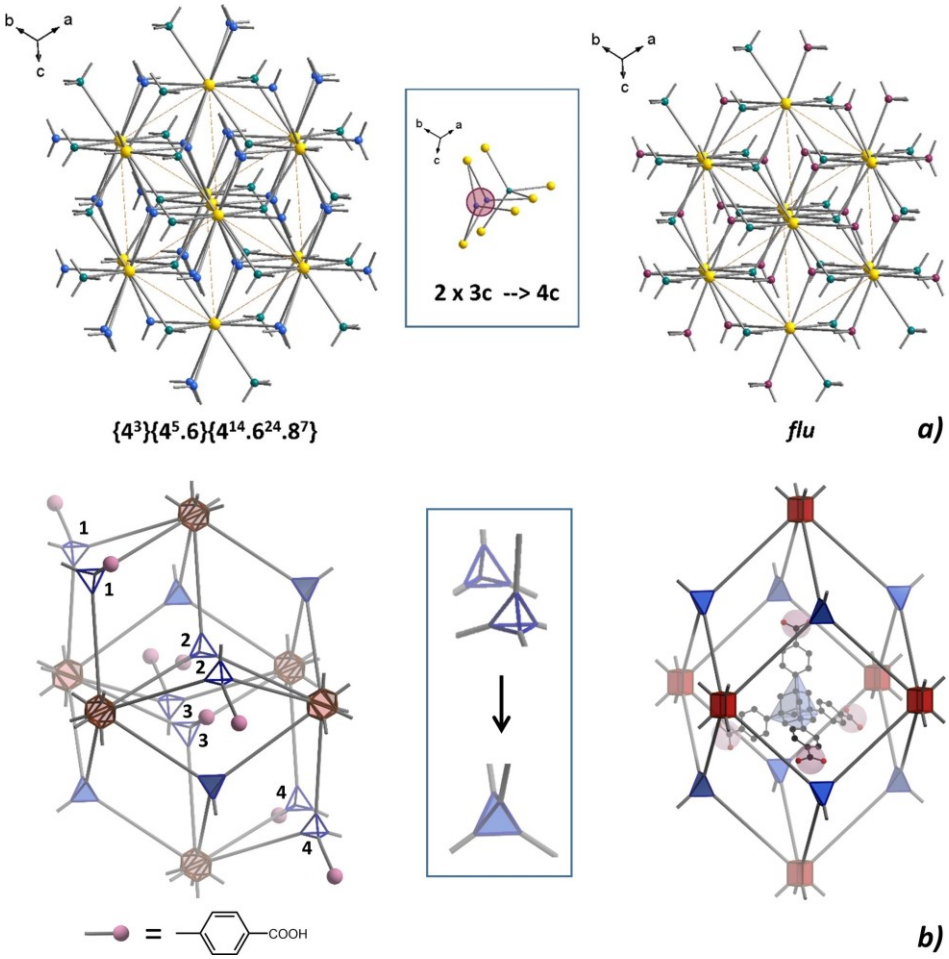

Fig. 6 The relation between the underlying net of **1** and the **flu** net: the topological equivalence by merging two three-connected nodes to one four-connected.
(a) Network representation.
(b) Related cages. The wireframe tetrahedron stands for the HL^{3-} and the filled tetrahedron for the L^{4-} ligand. The pink spheres designate the non-coordinated carboxy groups. The representation of the encapsulated H_4L^4 guest in a cage of the **flu** net is illustrative, without suggested localization.

The formal topological descriptors do not disclose the curious fact that the underlying net in **1** is related to the actually expected **flu** net *via* a simple transformation: pairs of metrically close 3-c nodes are merged to 4-c nodes *via* overlapping two out of the three edges (Fig. 6). Notably, **1** is not interpenetrated. High symmetry realizations of **flu** net, on its own, are known to be 'not-prone' to interpenetrate with its copies. It is a typical property of highly connected non-self-dual nets (the net, dual to **flu**, is **fcu**) in contrast to realizations of self-dual nets, like **srs**, **dia**, and **pcu**.[52,53] This feature of the **flu** net makes it a desirable target for reaching optimal porosity characteristics,[26] and the related **1** does not fail in this regard as well.

Probably the most interesting structural feature of **1** on the framework level is associated with the non-coordinated carboxyphenyl groups. The smallest distance between the *O*-atoms of the close pairs is only 4.69 Å from each other (Fig. 5b). The method of preparation of **1** included

a large amount of formic acid as a modulator, ensuring the non-deprotonation. The region between the close carboxy-functions contains only weak residual electron density peaks, precluding the presence of zirconium, but suggesting partial occupancy of the area by H-bonded species (see SI.2). The structure of **1** should favor the post-synthetic introduction of a coordination-bonded cluster with tailorable catalytic functions, using the carboxy functions as anchors.

Table 1. Summary on the topology and porosity related data for **1** and **2**. The respective data for the known MOF-841 and PCN-521 are listed for comparison.

Compd.	Framework composition; space group; {point symbol}; RCSR code[a]	Surface area, experimental (calculated) [b] / $m^2\ g^{-1}$	Void volume part, experimental (calculated) [c] / $cm^3\ cm^{-3}$	Max. included / max. free probe diameter; [d] / Å	Density of the desolvated framework, calculated / $g\ cm^{-3}$
1	$[Zr_6(\mu_3\text{-}O)_4(\mu_3\text{-}OH)_4(L^4)(HL^4)_2(OH)_2(H_2O)_2]$; C*2/c*; 3,4,10-c net; $\{4^{14}.6^{24}.8^7\}\{4^3\}_2\{4^5.6\}$; **-**	1190 for **1´**, (1886)	0.463 (0.576)	8.9, 5.3	0.906
2	I*4/m*; 8-c $[Zr_6(\mu_3\text{-}O)_4(\mu_3\text{-}OH)_4(OH)_4(L^4)_2(H_2O)_4]$; $\{4^{12}.6^{12}.8^4\}\{4^6\}_2$; **flu**	[585 for **2´**] [e] , (3197)	[0.261] [e] (0.718)	15.8, 6.6	[0.860] [e] ~0.63
MOF-841 lit. [30]	$[Zr_6(\mu_3\text{-}O)_4(\mu_3\text{-}OH)_4(MTB)_2(HCOO)_4(H_2O)_4]$, $\{4^{12}.6^{12}.8^4\}\{4^6\}_2$, **flu**	1390 (2078.11)	(0.631)	11.2, 5.9	0.914
PCN-521, lit. [26]	$[Zr_6(\mu_3\text{-}OH)_8(OH)_8(MTBC)_2]$, $\{4^{12}.6^{12}.8^4\}\{4^6\}_2$; **flu**	3411 (4167)	(0.795)	19.4, 8.6	0.449

[a] The RCSR (Reticular Chemistry Structure Resource) code is a unique net identifier. [54]

[b] Connoly surface area calculated by Monte-Carlo method employing a probe with 3.681 Å diameter. [55] The SCXRD structural data were used for experimental structures with removed solvent molecules, including the terminally coordinated ones. The disordered parts of the molecules were 'collapsed'.

[c] Experimental Gurvich pore volume at P/P0 = 0.95; calculated pore volume by SOLV/PLATON (probe diameter of 2.4 Å). [56]

[d] Maximal diameter of a spherical probe, which could be included in the framework (*i.e.* hosted in it) and the maximal diameter of the spherical probe, which could pass along a thorough-channel.[57]

[e] The formally assigned experimental data for **2´** (1-HCOOH-190C sample), which is interpreted as $[Zr_6(\mu_3\text{-}O)_4(\mu_3\text{-}OH)_4(OH)_4(L^4)_2] \cdot H_4L^4$.

$[Zr_6(\mu_3\text{-}O)_4(\mu_3\text{-}OH)_4(OH)_4(L^4)_2] \cdot H_4L^4$; 2´ (phase II). The degassing of compound **1** in vacuum under heating (Fig. 3), which aimed a preparation for a routine sorption measurement, caused a phase transition, resulting in **2´** (**ZRTE-11** §). The transformation takes place in-between 120C-190 °C, and the process was evidently concomitant with the complete removal of the guest solvent molecules. The product of the transition possesses a peculiar PXRD pattern with only two remarkably sharp peaks and nearly no other details (Fig 8). The absence of fine detail is not surprising, taking into account the inevitable decrease of crystallinity: the low-temperature solid state transition does not allow efficient defect-healing. The low number of strong peaks suggested that the formed crystalline compound has a structure of high symmetry. The evident candidate for phase II is the expected structure with

the **flu** underlying net. In this case the phase transition of I to II under heating could be interpreted as a conversion of an intermediary product, stabile at a lower temperature, to a more symmetric final product.

The interpretation of the phase transition is complicated by the fact that the stoichiometry of the nets are different: Zr : H_nL^4 is 1 : 3 for **1** and 1 : 2 for the expected compound with the **flu** underlying net. During such conversion 1/3 of the ligands should be expelled from the framework into the pores. While the formed ligand could be hosted in the formed highly porous structure with large inner cavities (~16 Å diameter max. cavity; the relative size of the ligand is given faithfully in Fig. 6b) the process of the framework's re-assembly did not proceed smoothly, which is evident from the somewhat decreased crystallinity (absence of weak peaks in the PXRD pattern).

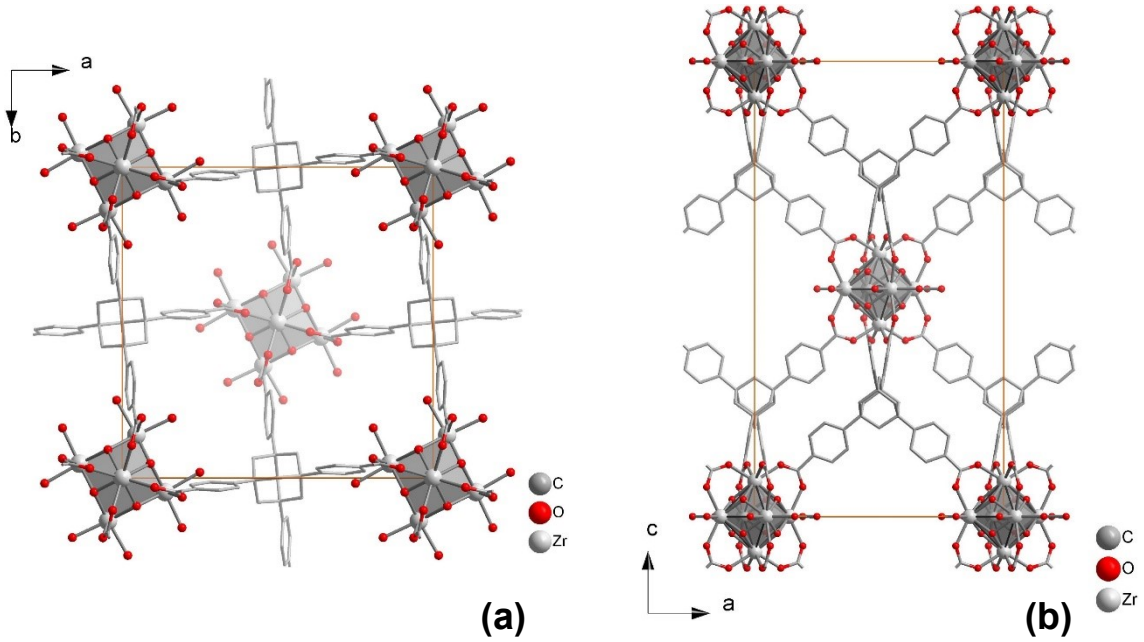

Fig. 7 The structural model of $[Zr_6(\mu_3\text{-}O)_4(\mu_3\text{-}OH)_4(OH)_4(L^4)_2]$, **2** with a **flu** underlying net; a) view along c axis b) view along b axis.

The decrease of crystallinity of **2´** under phase transition poses a critical problem for structural determination. Either a single crystal XRD determination or a Rietveld refinement based on two peaks is not realistic. However, the high-quality PXRD data allowed us at least to verify the hypothesis regarding the structure of **2** · H_4L^4. For that, a structural model of **2** (*I*4/m) was created, using the structure of MOF-841 as a prototype (Fig. 7; the atomic coordinates are given in SI.4; note that the variant of the framework formula of **2** is given with maximal number of hydroxido ligands, which could convert to oxo ligands upon strong degassing). The refinement strategy, taking into account the featurelessness of the pattern, was to refine the two independent cell parameters and two profile parameters. The LeBail fit gave a satisfactory correspondence (wR_p = 0.052) with <2% change of the cell parameters

compared to the initial model, constructed geometrically. The subsequent Rietveld fitting revealed that the calculated pattern contained three strong peaks, with one of them having no correspondence in the experimental pattern (Fig. S11). In this case preferred orientation is of low probability, however the presence of the guest might have an influence on the relative intensities of the peaks. The placement of a model guest in the vicinity of (½, 0, 0) coordinate, which is in the middle of a void, diminished strongly the 'redundant' peak. Finally, the H_4L^4 guest molecule was modeled with three heavy atoms, arbitrarily chosen to be Zr atoms. The crude modeling approach for **2-Guest** still allowed to reach wR_p=0.15 (Fig. S12 for profile fitting and Fig. 8 and S11 for comparison of the simulated PXRDs with the experimental ones. For further details see SI.5; the cif files for the refined structure are given as supplementary files). That result should be viewed as a verification of the structural hypothesis regarding **2**, rather than full-fledged refinement. The latter is impossible due to inherent limitations in the quality of the PXRD data.

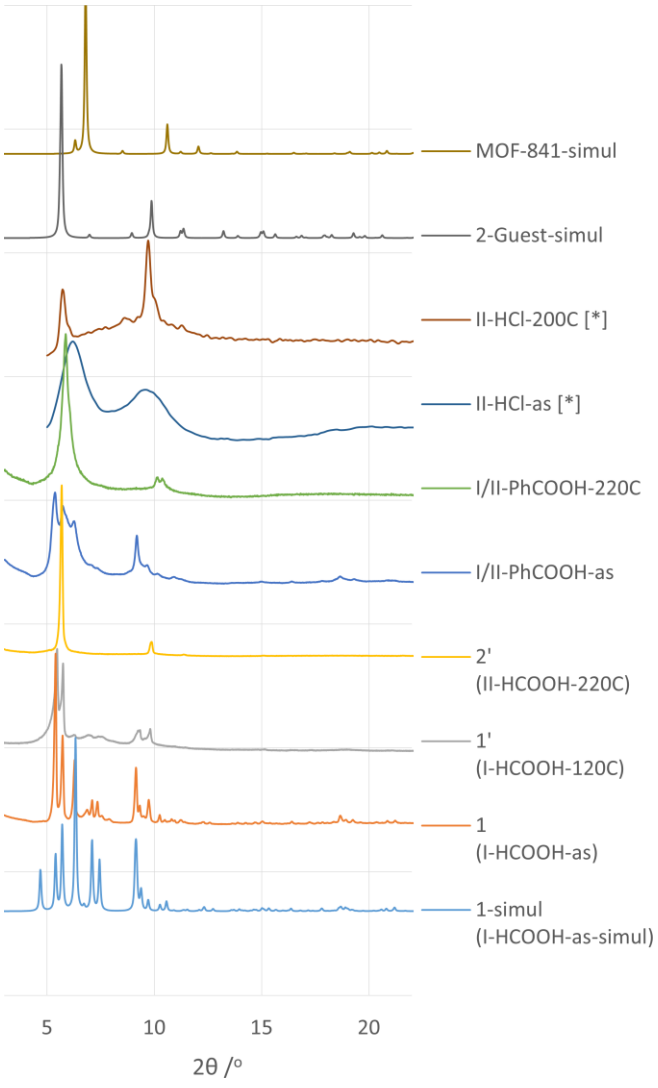

Fig. 8 The PXRD patterns of **1** and **2**, both experimental and simulated, and their comparison with the simulated pattern of MOF-841.
Note: the patterns marked by [*] are measured using a flat sample-holder reflectance mode, compared to the much more precise measurement in capillaries for other cases. A part of the broadening for the marked patterns could be attributed to the method of measurement.

The use of other modulators (phase I/II). The use modulators other than formic or acetic acids yielded mostly products of medium to poor crystallinity, even if the yields tend to be higher, up to ~80-90% in the case of HCl (Table 1). The PXRD patterns of these, typically semi-amorphous, materials, contained two very broad peaks (Fig. 8, on the example of I/II-HCl-as). The broad peaks are mostly, but not entirely overlapped with PXRD pattern of **1** (phase I) and entirely overlap with **2´** (phase II), being slightly closer to the latter. All these materials are classified as representing semi-amorphous mixed I/II phases (Fig. 3).

An interesting intermediary case and a partial exception is the I/II-PhCOOH-as, synthesized with benzoic acid as a modulator. While the sample was primarily represented by very small monocrystals, they diffracted very poorly. The maximal achievement in that regard was the indexing of a few particularly small crystals among dozens of attempted. The exception crystals turned out to be belonging to phase I (*i.e.* isostructural with **1**, Table S3). The PXRD pattern for the sample, isolated immediately after the synthesis, demonstrated significantly better crystallinity, compared to the very poor diffraction witnessed by the single crystal studies. We came to the conclusion, that under the temperature of synthesis (130 °C) another phase forms, but upon cooling it transforms to phase I in the mother liquor (rapid isolation decreases the speed of conversion significantly and allows to measure a 'mixed-phase' PXRD with a significant crystallinity). Unfortunately, we were not able to prove that the initially formed phase is identical to phase II. In any case, I/II-PhCOOH-as transforms to **2´** (Fig. S11) with quite good crystallinity upon heating, demonstrating an identical behavior to **1** in this respect.

All the I/II phases, except I/II-PhCOOH-as, are nearly amorphous in the as-synthesized form but improve their crystallinity upon heating at ~200 °C (the process could be viewed as a partial crystallization / aging). The strongest improvement was found for I/II-HCl-as (Fig. 8). The use of hydrochloric acid as a modulator ensures also high yield, which made the method interesting for the mixed ligand approach.

Semi-amorphous mixed ligand materials. The structure of **1**, with two out of three ligands acting as three-functional, endows the potential H_4L^4/H_3L^3 mixed ligand approach with a clear context. Indeed, **1** contains an $(HL^4)^{3-}$ ligand, which is functionally equivalent to the $(L^3)^{3-}$ ligand. Hence, an individual compound with a framework composition of $[Zr_6(\mu_3\text{-}O)_4(\mu_3\text{-}OH)_4(L^4)(L^3)_2(OH)_2(H_2O)_2]$ is structurally feasible. The analysis of the single crystal structure of **1** is encouraging in this regard; the non-coordinated branches of the $(HL^4)^{3-}$

ligand have large equivalent thermal displacement parameters. The disorder of the branches (see SI.2) only partially explains the effect. It is reasonable to assume that a part of the $(HL^4)^{3-}$ are substituted to $(L^3)^{3-}$, which is present as an additive. The independent refinement of the two disordered components gives an aggregate occupancy of ~0.96. In other words, around 4% of $(HL^4)^{3-}$ to $(L^3)^{3-}$ substitution rate is estimated from the structural data. This value is very approximative, but the high-quality of the SCXRD data give them certain weight. Nevertheless, the NMR spectra of the HF-digested sample (SI.8) did not show appreciable presence of H_3L^3 in a bulk sample.

A number of experiments with different initial H_3L^3 : H_4L^4 ratios aiming mixed-ligand Zr-PCPs were performed. With HCOOH and AcOH used as modulators, the yield and crystallinity dropped, when the content of H_3L^3 increased to amounts comparable to H_4L^4. At ~1 : 1 ratio the products were already non-crystalline. The NMR spectra of crystalline samples confirmed, that the inclusion of H_3L^3 is minimal at best. It could be, hence, concluded, that the role of H_3L^3 at low concentrations is limited to induction of the crystallization (it is worth noting that even the 'pure' H_4L^4 might contain trace amounts of H_3L^3 due to method of preparation. The "Newman's" protocol of benzene alkylation [48] yields a mixture of all the possible bridge-head functionalized adamantanes, starting from mono- to 1,3,5,7-tetraphenyladamantanes that are functionalized further). Under slow, controlled crystal-growth the much less soluble H_4L^4 is included in the product preferentially. The low-yields for these modulators were equivalent to a recrystallization, with harvesting the most pure, single-ligand product.

The inclusion of $(L^3)^{3-}$ is achievable for semi-armorphous samples. When 1 : 2 ratio of H_4L^4 : H_3L^3 is used, the NMR of the digested sample indicates a 1 : 0.64 ratio of the ligands in the product (Fig. S20; see Fig. S7 for the PXRD). The low yielding synthesis still causes enrichment of the product with H_4L^4.

The high yielding (up to ~80%) HCl-modulated synthesis turned to be the best suited for 'forcing' the incorporation of the H_3L^3. An amorphous model compound I/IId-mix-HCl-as was prepared by using H_4L^4 : H_3L^3 1 : 1 ratio; the incorporation of the ligand was confirmed by NMR (1 : 1.09 ratio in the product; Fig. S20) and comparative IR spectroscopy (Fig. S22). The primary motivation in making this model material, which crystallinity increases upon activation (Fig. S10), was the assessment of ligand substitution on the porosity characteristics, discussed below.

N_2 gas adsorption studies. The results on the adsorption studies and the found BET areas are summarized in Table 2. The preparation for low temperature degassing (120 °C) involved an acetone exchange with short exposition, followed by thorough supercritical CO_2 drying (sc-CO_2; 99 cycles / 7 h). The procedure allowed to remove nearly all the DMF, which was confirmed by IR spectroscopy (Fig. S21). **1´**, obtained by degassing of **1** (or its analogue,

prepared using acetic acid), is mostly retained the framework structure under the low temperature degassing (Fig. 8, first signs of conversion to **2´** after 24 h degassing in a capillary; Fig S8, typical 3 h degassing, less precise flat sample-holder measurement). The maximal surface area of 1190 $m^2 g^{-1}$ was registered, with little difference between materials synthesized using formic or acetic acid (Table 2, Fig. 9, S14). The simulated value for the solvent-free framework of **1´** is 1886 $m^2 g^{-1}$ (Table 1); the discrepancy might be explained by the decrease of crystallinity due to start of conversion to **2´** and presence of minor amounts of residual solvent. The converted structure of **2´** has a maximum observed porosity of 576 $m^2 g^{-1}$. It is only a fifth of the simulated value of for the idealized **2** with fluorite structure (**2´** ≡ **2** · H_4L^4). Evidently, the encapsulated ligand, which is expulsed to the pores during conversion, takes its toll. The ligand is larger than the vdW opening of the **flu** net cage; the openings have a lozenge shape with sides equal to ligand's branch, Fig. 6. Hence, no ligand's mobility was expected, especially because of the generally low solubility of the H_4L^4 ligand. The hypothesis was checked experimentally, but no increase of surface area was registered for **2** · H_4L^4 after soaking in DMF for two days and subsequent activation.

Table 2. Degassing conditions and observed surface areas.

Sample name	Degassing temp, °C	Sample pre-preatment	SBET, $m^2 g^{-1}$
I-HCOOH-120C or **1´**	120	sc-CO_2	1190
I-HCOOH-190C or **2´**	120	sc-CO_2	576
I-AcOH-120C	120	sc-CO_2	1126
I/II-PhCOOH-120C	120	sc-CO_2	763
I/II-HCl-200C	200	sc-CO_2	546
I/IId-mix-HCl-200C	200	-	452
I/IId-HCl-200C	200	-	396
I/II-TFA-120C	120	sc-CO_2	253
I/II-no-modul-200C	200	-	233

The semi-amorphous phases degassed at a low temperature (120 °C) demonstrated low surface areas, with the remarkable exception of the I/II-PhCOOH sample (762.5 $m^2 g^{-1}$). Composed of crystalline phase I at least partially, and demonstrating conversion to pure **2´**, I/II-PhCOOH is much closer to **1**, compared to the rest of I/II materials. However, the latter demonstrates a strong increase in crystallinity, when degassed at 200 °C. The best result is obtained for I/II-HCl-200C with 546 $m^2 g^{-1}$ surface area. This value is surprisingly close to the surface area of the much more crystalline **2´**. The thermal treatment at ~200 °C evidently 'equilibrates' the structures with a tendency to near the phase II-type structurally. The considerable surface area of the semi-amorphous I/II-HCl-200C might be explained by a lesser amount of the expulsed H_4L^4 ligand in the pores (indeed, the PXRD pattern of parent I/II-HCl-as corresponds slightly better to phase II than to I according to PXRD). The material prepared without a modulator, I/II-no-modul-200C, demonstrated the lowest surface area, indicating that the use of modulators has a beneficial effect in partial 'crystallization' at elevated temperatures.

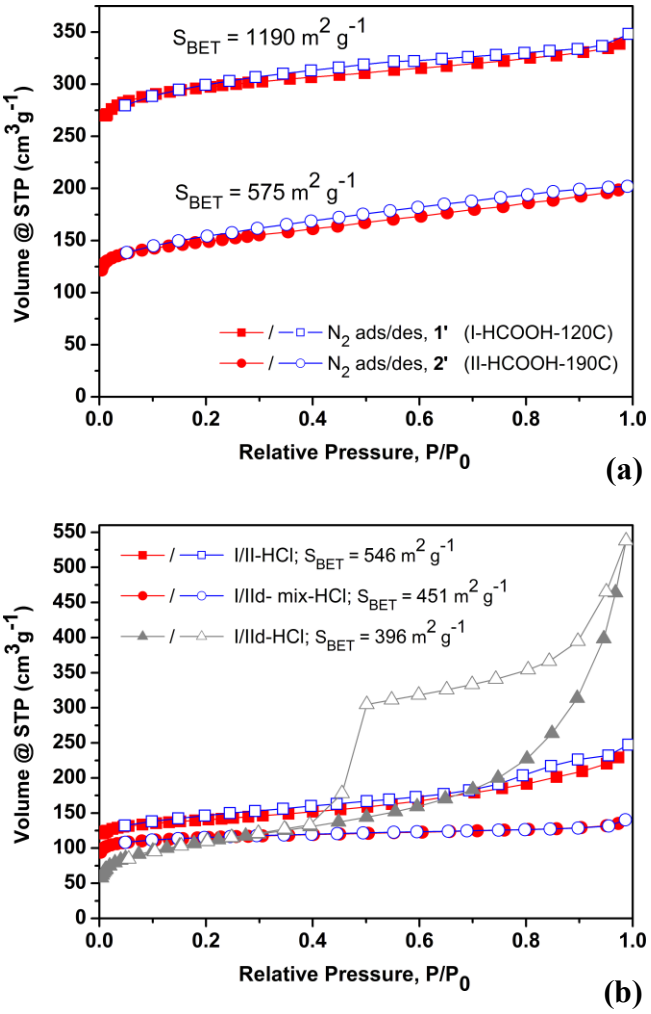

Fig. 9 N_2 gas adsorption isotherms. a) **1**-HCOOH after sc-CO_2 drying followed by activation at 120 °C and the same sample after activation at 190 °C, causing conversion to phase **2**. b) Semi-amorphous samples obtained for H_4L^4 only (top legend line), mixture of H_4L^4/H_3L^3 1:1 (middle), and with H_3L^3 only (bottom).

The mixed-ligand material, I/IId-mix-HCl-200C had a surface area of 452 m^2 g^{-1}, which is right in-between the values for I/II-HCl-200C and I/IId-HCl-200C materials, based on pure H_4L^4 and H_3L^3 respectively (400-550 m^2 g^{-1}). Even if the increase of H_3L^3 share expectedly decreased the surface area, the moderate influence confirms, that H_3L^3 functions similarly to H_4L^4. However, there is an interesting distinction from the H_3L^3-only based material. Unlike the H_4L^4- or mixed-ligand based materials with adsorption isotherm characteristic for microporous solids (Type I isotherm, IUPAC classification), the H_3L^3-only based material demonstrates a strong and distinctive mesoporosity with a very pronounced, large hysteresis (Type IV; Fig 9b). It could be interpreted the next way: the ‘truncation’ of one ‘branch’ of the H_4L^4 decreases the local order (crystallinity), which is associated with high microporosity;

however, the 'truncation' creates more defects, which translates in larger mesoporosity. The result bears an interesting similarity to mostly amorphous covalent organic framework materials, based on tris- and tetrakis- adamantanes,[58] where no dramatic difference exists between the two (even if larger values could be predicted for the tetrahedral building blocks due to possible realization of highly symmetric periodic structures).

Water stability. **1′** and **2′** were subjected to water stability tests. The degassed samples were left in contact with water for 1 day at room temperature and for 1 h at 100 °C. The treatment at room temperature showed some deterioration of the crystallinity of **1′** with a clear tendency of commencing the transition to **2′** and no changes in crystallinity of **2′** (Fig. S23). The treatment in boiling water caused complete transition of **1′** to **2′** with a crystallinity not visibly different from the initial sample of **2′**, or **2′** treated with boiling water. As for the actual surface areas (Tab. S4) the treatment in water even at room temperature causes a drop for approximately four times, with a further decrease after treatment in boiling water. Thus, the water stability of the synthesized materials is low. The most remarkable observation is that water stimulates the conversion of **1′** to **2′** at significantly lower temperatures than it is observed in the solid state.

Conclusions

The Zr-PCP/MOF structure of **1** features a highly symmetric tetrahedral ligand and yet, unexpectedly, it is of low-symmetry (*C*2/c). The structure, based on an unusual 10 connected Zr_6 cluster, have a significant proven porosity (up to 1190 $m^2\ g^{-1}$) and is in a number of ways remarkable. The mono-deprotonated HL^4 ligand in the $[Zr_6(\mu_3\text{-}O)_4(\mu_3\text{-}OH)_4(L^4)(HL^4)_2(OH)_2(H_2O)_2]$ framework is equivalent to a tri-functionalized 'truncated' tetrahedral ligand. Such structural organization allows the introduction of a bulky functionality instead of the non-involved carboxyphenyl moiety. Alternatively, the non-involved carboxy groups, protruding inside the cavities and nearly meeting with each other, are suitable for postsynthetic anchoring of functional entities, particularly for building-up coordination-bonded clusters.

The conversion of **1** to the expected **flu** structure of **2′** with higher symmetry (*I*4/m) takes place at a relatively low temperature (<190 °C) in vacuum. It is a relatively rare phase transition for PCPs, as it undergoes in the solid state (no solvent assistance) and is accompanied with expulsion of a ligand (notably, the conversion also takes place in the presence of water, very slowly at near room temperatures and fast at 100 °C). The latter is hosted in the pores of the structure, and **2′** is an inclusion compound with $[Zr_6(\mu_3\text{-}O)_4(\mu_3\text{-}OH)_4(OH)_4(L^4)_2] \cdot H_4L^4$ formula (the ligand is geometrically larger than the vdW size of the pore openings). The solid-state network rearrangement with ligand expulsion in the pores is a potential method for encapsulation of functional entities, superior to the simpler 'ship-in-the-bottle' synthesis.

Interestingly, the complex three-nodal topology of **1** and the **flu** topology of **2´** are related. The imaginary transformation that makes them equivalent is the merge of certain three-connected node pairs in a single four-connected node by making two pairs of edges common (the node pairs are close in the structure, which might explain the facility of the transformation). The structure of **1** could be viewed as a 'defect'-structure, but in an unusual, inversed way: it contains an excess of ligands and the thermally induced phase transition 'heals' the structure (the 'standard' PCP/MOFs defects are associated with lack of ligands).

The attempt to synthesize a pure crystalline analog of **1** with the trifunctional L^3 'truncated' ligand equivalent to HL^4 was not successful. The best quality crystals were enriched by H_4L^4 compared to H_3L^3, seemingly due to high solubility difference (it might be a lesser issue in the case of potential functionalized H_3RL^3 ligands). However, the mixed ligand approach was successful for semi-amorphous products, which could be obtained in high yields using HCl as a modulator. The semi-amorphous PCP-gels increase their crystallinity upon thermal treatment and demonstrate close porosities of 400-550 $m^2\ g^{-1}$ when synthesized using pure ligands or their mixtures alike. The structures of the partially crystallized gels (Phase I/II) could be regarded as composed of domains corresponding to frameworks of **1** and **2** according to the intermediary nature of the respective PXRD patterns.

Acknowledgements

R.B acknowledges the funding by "Intelligent Design of Nanoporous Adsorbents and Catalysts" no. P106/12/G015 from the Czech Science Foundation, and C.J. expresses his gratitude for the support by Optimat 03SF0492C grant from the Federal German Ministry of Education and Research (BMBF). The authors are grateful to Dr. Michal Dusek and Dr. Pavel Macek from the Academy of Sciences of the Czech Republic for respectively organizing and carrying out the high-quality PXRD capillary measurements. Dr. Tobias Stürzer and Holger Ott from Bruker AXS GmbH are acknowledged for their effort in testing the identity of the I/II-PhCOOH-as sample with the newest state-of-art single crystal diffractometer.

§ - The code names ZRTE-10 for **1'** and ZRTE-11 for **2'** materials are used for the convenience of external referencing only (the code is generic; ZR-stands for zirconium and TE for the tetrahedral ligand). The internal naming system is two-fold. The primary compounds are named **1, 1', 2** and **2'** (The **'** suffix designates the experimental degassed forms containing no volatile guests; **2** is the idealized framework, **2'** ≡ **2**·H_4L^4**)**. The secondary materials are referred using a general sample code, *Phase[d][-mix]-Modulator-Condition*, where: *Phase* = {I, II, I/II}, the actual phase-type; *[d]*, optional suffix designating the use of H_3L^3 (otherwise H_4L^4 is implied); *[-mix]* – optional suffix, for the use of H_3L^3 + H_4L^4; *Modulator* = {HCOOH, AcOH, PhCOOH, HCl, TFA, no-modul}; *Condition* = {as,

temperature}, where 'as' stands for as-synthesized and 'temperature' is the temperature in Celsius, e.g. '120C'. For example, I-HCOOH-as (which is equivalent to **1**) means the as-synthesized sample of phase I type, synthesized using HCOOH as a modulator.

‖ Synthesis, a short description (complete information is given in the Supplementary Information):
1: A solution of 42 mg of $ZrOCl_2 \cdot 8H_2O$ and 22 mg of H_4L^4 in 4.60 ml of DMF and 2.64 ml of HCOOH was heated at 130 °C for 96 h in a sealed culture tube (note, 3% of H_3L^3 as an additive to H_4L^4 was used in repeated syntheses, see SI.1). The product, consisting of small single-crystals was filtered off, washed with DMF acetone and dried in air until permanent weight. Yield: 9 mg (18%). When acetic acid is used, the yield of 1-AcOH-as was 20.2 mg (~40%).
1′: **1**, after sc-CO_2 drying (see SI.7), was heated in vacuum (10^{-3} mbar) at 120 °C, for 3 h.
2′: **1** was heated in vacuum (10^{-3} mbar) at 220 °C for 3 h.
I/II-HCl-as: 19 mg of $ZrCl_4$ and 20 mg of H_4L^4in 2.5 ml of DMF and 0.17 ml of HCl were heated at 120 °C for 24 h in a sealed culture tube. The white gel-like product was washed by DMF and acetone followed by drying in air until permanent weight. The yield of the white solid was 31 mg (74% approx.).

& Selected crystal data for **1**: $C_{114}H_{96}O_{36}Zr_6$ (framework only), FW =2589.34, monoclinic, *C2/c.* a = 24.261(5) Å, b = 30.967(6) Å, c =25.454(5) Å, β =101.91(3) V = 18712(7) Å^3 Z = 4, R1[$F^2 > 2\sigma(F^2)$] = 0.0341. CCDC reference number is 1921424. The crystallographic data in CIF format could be downloaded free of charge at https://www.ccdc.cam.ac.uk/-structures/. **2-Guest** (**2** · H_4L^4): $C_{80}H_{64}O_{32}Zr_{12.8}$ (note: the H_4L^4 guest molecule was modeled by a few Zr atoms) FW = 1352.5, tetragonal, *I*4/m, a = 17.9142 was c = 31.5291 V = 10118.3 Å^3, Z = 2, wR_p = 0.155. The supplementary information contains also the data on I-AcOH-as, isostructural to **1**.

Supporting Information

Detailed synthetic descriptions, SCXRD crystal data and refinement for **1** as well as for its variants, topological description of **1**, PXRD based model of **2** and refinement details, TGA, gas adsorption data, ^{1}H NMR spectra, and FT-IR spectra.

References

(1) Bai, Y.; Dou, Y.; Xie, L.-H.; Rutledge, W.; Li, J.-R.; Zhou, H.-C. Zr-Based Metal–Organic Frameworks: Design, Synthesis, Structure, and Applications. *Chem. Soc. Rev.* **2016**, *45*, 2327–2367.
(2) Lu, W.; Yuan, D.; Makal, T. A.; Wei, Z.; Li, J.-R.; Zhou, H.-C. Highly Porous Metal-Organic Framework Sustained with 12-Connected Nanoscopic Octahedra. *Dalton Trans.* **2013**, *42*, 1708–1714.
(3) Li, B.; Wen, H.-M.; Zhou, W.; Chen, B. Porous Metal–Organic Frameworks for Gas

Storage and Separation: What, How, and Why? *J. Phys. Chem. Lett.* **2014**, *5*, 3468–3479.
(4) Wang, Y.; Zhao, D. Beyond Equilibrium: Metal–Organic Frameworks for Molecular Sieving and Kinetic Gas Separation. *Cryst. Growth Des.* **2017**, *17*, 2291–2308.
(5) Wang, B.; Lv, X.-L.; Feng, D.; Xie, L.-H.; Zhang, J.; Li, M.; Xie, Y.; Li, J.-R.; Zhou, H.-C. Highly Stable Zr(IV)-Based Metal–Organic Frameworks for the Detection and Removal of Antibiotics and Organic Explosives in Water. *J. Am. Chem. Soc.* **2016**, *138*, 6204–6216.
(6) Xie, L.-H.; Liu, X.-M.; He, T.; Li, J.-R. Metal-Organic Frameworks for the Capture of Trace Aromatic Volatile Organic Compounds. *Chem* **2018**, *4*, 1911–1927.
(7) Wu, M.-X.; Yang, Y.-W. Metal-Organic Framework (MOF)-Based Drug/Cargo Delivery and Cancer Therapy. *Adv. Mater.* **2017**, *29*, 1606134.
(8) Lee, J.; Farha, O. K.; Roberts, J.; Scheidt, K. A.; Nguyen, S. T.; Hupp, J. T. Metal-Organic Framework Materials as Catalysts. *Chem. Soc. Rev.* **2009**, *38*, 1450–1459.
(9) Huang, Y.-B.; Liang, J.; Wang, X.-S.; Cao, R. Multifunctional Metal–Organic Framework Catalysts: Synergistic Catalysis and Tandem Reactions. *Chem. Soc. Rev.* **2017**, *46*, 126–157.
(10) Liu, J.; Chen, L.; Cui, H.; Zhang, J.; Zhang, L.; Su, C.-Y. Applications of Metal–Organic Frameworks in Heterogeneous Supramolecular Catalysis. *Chem. Soc. Rev.* **2014**, *43*, 6011–6061.
(11) Zhang, T.; Lin, W. Metal–Organic Frameworks for Artificial Photosynthesis and Photocatalysis. *Chem. Soc. Rev.* **2014**, *43*, 5982–5993.
(12) Sun, D.; Li, Z. Robust Ti- and Zr-Based Metal-Organic Frameworks for Photocatalysis. *Chinese J. Chem.* **2017**, *35*, 135–147.
(13) Lustig, W. P.; Mukherjee, S.; Rudd, N. D.; Desai, A. V.; Li, J.; Ghosh, S. K. Metal–Organic Frameworks: Functional Luminescent and Photonic Materials for Sensing Applications. *Chem. Soc. Rev.* **2017**, *46*, 3242–3285.
(14) Stavila, V.; Talin, A. A.; Allendorf, M. D. MOF-Based Electronic and Opto-Electronic Devices. *Chem. Soc. Rev.* **2014**, 5994–6010.
(15) Garibay, S. J.; Cohen, S. M. Isoreticular Synthesis and Modification of Frameworks with the UiO-66 Topology. *Chem. Commun.* **2010**, *46*, 7700–7702.
(16) Cmarik, G. E.; Kim, M.; Cohen, S. M.; Walton, K. S. Tuning the Adsorption Properties of UiO-66 via Ligand Functionalization. *Langmuir* **2012**, *28*, 15606–15613.
(17) Biswas, S.; Van Der Voort, P. A General Strategy for the Synthesis of Functionalised UiO-66 Frameworks: Characterisation, Stability and CO 2 Adsorption Properties. *Eur. J. Inorg. Chem.* **2013**, *2013*, 2154–2160.
(18) Ragon, F.; Campo, B.; Yang, Q.; Martineau, C.; Wiersum, A. D.; Lago, A.; Guillerm, V.; Hemsley, C.; Eubank, J. F.; Vishnuvarthan, M.; Taulelle, F.; Horcajada, P.; Vimont, A.; Llewellyn, P. L.; Daturi, M.; Devautour-Vinot, S.; Maurin, G.; Serre, C.; Devic, T.; Clet, G. Acid-Functionalized UiO-66(Zr) MOFs and Their Evolution after Intra-Framework Cross-Linking: Structural Features and Sorption Properties. *J. Mater. Chem. A* **2015**, *3*, 3294–3309.
(19) Manna, K.; Zhang, T.; Greene, F. X.; Lin, W. Bipyridine- and Phenanthroline-Based Metal–Organic Frameworks for Highly Efficient and Tandem Catalytic Organic Transformations via Directed C–H Activation. *J. Am. Chem. Soc.* **2015**, *137*, 2665–2673.
(20) Chen, T.-H.; Popov, I.; Miljanić, O. Š. A Zirconium Macrocyclic Metal-Organic Framework with Predesigned Shape-Persistent Apertures. *Chem. - A Eur. J.* **2017**, *23*, 286–290.
(21) Eddaoudi, M.; Kim, J.; Rosi, N.; Vodak, D.; Wachter, J.; O'Keeffe, M.; Yaghi, O. M.

Systematic Design of Pore Size and Functionality in Isoreticular MOFs and Their Application in Methane Storage. *Science* **2002**, *295*, 469–472.
(22) Deng, H.; Grunder, S.; Cordova, K. E.; Valente, C.; Furukawa, H.; Hmadeh, M.; Gándara, F.; Whalley, A. C.; Liu, Z.; Asahina, S.; Kazumori, H.; O'Keeffe, M.; Terasaki, O.; Stoddart, J. F.; Yaghi, O. M. Large-Pore Apertures in a Series of Metal-Organic Frameworks. *Science* **2012**, *336*, 1018–1023.
(23) Feng, D.; Wang, K.; Wei, Z.; Chen, Y.-P.; Simon, C. M.; Arvapally, R. K.; Martin, R. L.; Bosch, M.; Liu, T.-F.; Fordham, S.; Yuan, D.; Omary, M. A.; Haranczyk, M.; Smit, B.; Zhou, H.-C. Kinetically Tuned Dimensional Augmentation as a Versatile Synthetic Route towards Robust Metal–Organic Frameworks. *Nat. Commun.* **2014**, *5*, 5723.
(24) Zhai, Q.-G.; Bu, X.; Mao, C.; Zhao, X.; Daemen, L.; Cheng, Y.; Ramirez-Cuesta, A. J.; Feng, P. An Ultra-Tunable Platform for Molecular Engineering of High-Performance Crystalline Porous Materials. *Nat. Commun.* **2016**, *7*, 13645.
(25) Liu, T.-F.; Feng, D.; Chen, Y.-P.; Zou, L.; Bosch, M.; Yuan, S.; Wei, Z.; Fordham, S.; Wang, K.; Zhou, H.-C. Topology-Guided Design and Syntheses of Highly Stable Mesoporous Porphyrinic Zirconium Metal–Organic Frameworks with High Surface Area. *J. Am. Chem. Soc.* **2015**, *137*, 413–419.
(26) Zhang, M.; Chen, Y.-P.; Bosch, M.; Gentle, T.; Wang, K.; Feng, D.; Wang, Z. U.; Zhou, H.-C. Symmetry-Guided Synthesis of Highly Porous Metal-Organic Frameworks with Fluorite Topology. *Angew. Chem. Int. Ed. Engl.* **2014**, *53*, 815–818.
(27) Feng, D.; Gu, Z.-Y.; Li, J.-R.; Jiang, H.-L.; Wei, Z.; Zhou, H.-C. Zirconium-Metalloporphyrin PCN-222: Mesoporous Metal-Organic Frameworks with Ultrahigh Stability as Biomimetic Catalysts. *Angew. Chemie Int. Ed.* **2012**, *51*, 10307–10310.
(28) Feng, D.; Chung, W.-C.; Wei, Z.; Gu, Z.-Y.; Jiang, H.-L.; Chen, Y.-P.; Darensbourg, D. J.; Zhou, H.-C. Construction of Ultrastable Porphyrin Zr Metal–Organic Frameworks through Linker Elimination. *J. Am. Chem. Soc.* **2013**, *135*, 17105–17110.
(29) Jiang, H.-L.; Feng, D.; Wang, K.; Gu, Z.-Y.; Wei, Z.; Chen, Y.-P.; Zhou, H.-C. An Exceptionally Stable, Porphyrinic Zr Metal–Organic Framework Exhibiting PH-Dependent Fluorescence. *J. Am. Chem. Soc.* **2013**, *135*, 13934–13938.
(30) Queen, W. L.; Hudson, M. R.; Jiang, J.; Yaghi, O. M.; Gándara, F.; Furukawa, H.; Zhang, Y. Water Adsorption in Porous Metal–Organic Frameworks and Related Materials. *J. Am. Chem. Soc.* **2014**, *136*, 4369–4381.
(31) Feng, D.; Wang, K.; Su, J.; Liu, T.-F.; Park, J.; Wei, Z.; Bosch, M.; Yakovenko, A.; Zou, X.; Zhou, H.-C. A Highly Stable Zeotype Mesoporous Zirconium Metal-Organic Framework with Ultralarge Pores. *Angew. Chemie Int. Ed.* **2015**, *54*, 149–154.
(32) Ma, J.; Wong-Foy, A. G.; Matzger, A. J. The Role of Modulators in Controlling Layer Spacings in a Tritopic Linker Based Zirconium 2D Microporous Coordination Polymer. *Inorg. Chem.* **2015**, *54*, 4591–4593.
(33) Feng, D.; Jiang, H.-L.; Chen, Y.-P.; Gu, Z.-Y.; Wei, Z.; Zhou, H.-C. Metal–Organic Frameworks Based on Previously Unknown Zr 8 /Hf 8 Cubic Clusters. *Inorg. Chem.* **2013**, *52*, 12661–12667.
(34) Guillerm, V.; Ragon, F.; Dan-Hardi, M.; Devic, T.; Vishnuvarthan, M.; Campo, B.; Vimont, A.; Clet, G.; Yang, Q.; Maurin, G.; Férey, G.; Vittadini, A.; Gross, S.; Serre, C. A Series of Isoreticular, Highly Stable, Porous Zirconium Oxide Based Metal-Organic Frameworks. *Angew. Chemie* **2012**, *124*, 9401–9405.
(35) Taddei, M. When Defects Turn into Virtues: The Curious Case of Zirconium-Based Metal-Organic Frameworks. *Coord. Chem. Rev.* **2017**, *343*, 1–24.
(36) Shearer, G. C.; Chavan, S.; Bordiga, S.; Svelle, S.; Olsbye, U.; Lillerud, K. P. Defect Engineering: Tuning the Porosity and Composition of the Metal-Organic Framework UiO-66 via Modulated Synthesis. *Chem. Mater.* **2016**, *28*, 3749–3761.

(37) Katz, M. J.; Brown, Z. J.; Colón, Y. J.; Siu, P. W.; Scheidt, K. a; Snurr, R. Q.; Hupp, J. T.; Farha, O. K. A Facile Synthesis of UiO-66, UiO-67 and Their Derivatives. *Chem. Commun. (Camb).* **2013**, *49*, 9449–9451.
(38) Nguyen, H. G. T.; Schweitzer, N. M.; Chang, C.-Y.; Drake, T. L.; So, M. C.; Stair, P. C.; Farha, O. K.; Hupp, J. T.; Nguyen, S. T. Vanadium-Node-Functionalized UiO-66: A Thermally Stable MOF-Supported Catalyst for the Gas-Phase Oxidative Dehydrogenation of Cyclohexene. *ACS Catal.* **2014**, *4*, 2496–2500.
(39) Hu, Z.; Zhao, D. Metal–Organic Frameworks with Lewis Acidity: Synthesis, Characterization, and Catalytic Applications. *CrystEngComm* **2017**, *19*, 4066–4081.
(40) Jiang, J.; Gándara, F.; Zhang, Y.-B.; Na, K.; Yaghi, O. M.; Klemperer, W. G. Superacidity in Sulfated Metal–Organic Framework-808. *J. Am. Chem. Soc.* **2014**, *136*, 12844–12847.
(41) Zhu, L.; Liu, X.-Q.; Jiang, H.-L.; Sun, L.-B. Metal–Organic Frameworks for Heterogeneous Basic Catalysis. *Chem. Rev.* **2017**, *117*, 8129–8176.
(42) Dhakshinamoorthy, A.; Asiri, A. M.; Garcia, H. Metal–Organic Frameworks Catalyzed C–C and C–Heteroatom Coupling Reactions. *Chem. Soc. Rev.* **2015**, *44*, 1922–1947.
(43) Dhakshinamoorthy, A.; Garcia, H. Metal–Organic Frameworks as Solid Catalysts for the Synthesis of Nitrogen-Containing Heterocycles. *Chem. Soc. Rev.* **2014**, *43*, 5750–5765.
(44) Dhakshinamoorthy, A.; Opanasenko, M.; Čejka, J.; Garcia, H. Metal Organic Frameworks as Heterogeneous Catalysts for the Production of Fine Chemicals. *Catal. Sci. Technol.* **2013**, *3*, 2509–2540.
(45) Xu, T.; Hou, X.; Wang, Y.; Zhang, J.; Zhang, J.; Liu, B. A Gigantic Polyoxozirconate with Visible Photoactivity. *Dalt. Trans.* **2017**, *46*, 10185–10188.
(46) Zhao, T.; Heering, C.; Boldog, I.; Domasevitch, K. V.; Janiak, C. A View on Systematic Truncation of Tetrahedral Ligands for Coordination Polymers. *CrystEngComm* **2017**, *19*, 776–780.
(47) Liu, J.; Wang, W.; Luo, Z.; Li, B.; Yuan, D. Microporous Metal–Organic Framework Based on Ligand-Truncation Strategy with High Performance for Gas Adsorption and Separation. *Inorg. Chem.* **2017**, *56*, 10215–10219.
(48) Newman, H. Facile Syntheses of 1,3-Diphenyl-, 1,3,5-Triphenyl-, and 1,3,5,7-Tetraphenyladamantane from 1-Bromoadamantane. *Synthesis (Stuttg).* **1972**, *1972*, 692–693.
(49) Bon, V.; Senkovska, I.; Baburin, I. A.; Kaskel, S. Zr- and Hf-Based Metal–Organic Frameworks: Tracking Down the Polymorphism. *Cryst. Growth Des.* **2013**, *13*, 1231–1237.
(50) Ma, J.; Tran, L. D.; Matzger, A. J. Toward Topology Prediction in Zr-Based Microporous Coordination Polymers: The Role of Linker Geometry and Flexibility. *Cryst. Growth Des.* **2016**, *16*, 4148–4153.
(51) Zhang, X.; Zhang, X.; Johnson, J. A.; Chen, Y.-S.; Zhang, J. Highly Porous Zirconium Metal–Organic Frameworks with β-UH 3 -like Topology Based on Elongated Tetrahedral Linkers. *J. Am. Chem. Soc.* **2016**, *138*, 8380–8383.
(52) Bonneau, C.; O'Keeffe, M. High-Symmetry Embeddings of Interpenetrating Periodic Nets. Essential Rings and Patterns of Catenation. *Acta Crystallogr. Sect. A Found. Adv.* **2015**, *71*, 82–91.
(53) Friedrichs, O. D.; O'Keeffe, M.; Yaghi, O. M. The CdSO4, Rutile, Cooperite and Quartz Dual Nets: Interpenetration and Catenation. *Solid State Sci.* **2003**, *5*, 73–78.
(54) O'Keeffe, M.; Peskov, M. A.; Ramsden, S. J.; Yaghi, O. M. The Reticular Chemistry Structure Resource (RCSR) Database of, and Symbols for, Crystal Nets. *Acc. Chem.*

Res. **2008**, *41*, 1782–1789.
(55) Düren, T.; Millange, F.; Férey, G.; Walton, K. S.; Snurr, R. Q. Calculating Geometric Surface Areas as a Characterization Tool for Metal−Organic Frameworks. *J. Phys. Chem. C* **2007**, *111*, 15350–15356.
(56) Spek, A. L. PLATON SQUEEZE: A Tool for the Calculation of the Disordered Solvent Contribution to the Calculated Structure Factors. *Acta Crystallogr. Sect. C Struct. Chem.* **2015**, *71*, 9–18.
(57) Willems, T. F.; Rycroft, C. H.; Kazi, M.; Meza, J. C.; Haranczyk, M. Algorithms and Tools for High-Throughput Geometry-Based Analysis of Crystalline Porous Materials. *Microporous Mesoporous Mater.* **2012**, *149*, 134–141.
(58) Bhunia, A.; Boldog, I.; Möller, A.; Janiak, C. Highly Stable Nanoporous Covalent Triazine-Based Frameworks with an Adamantane Core for Carbon Dioxide Sorption and Separation. *J. Mater. Chem. A* **2013**, *1*, 14990–14999.